Amphibious Polymer Materials with High Strength and Superb Toughness in Various Aquatic and Atmospheric Environments

Hongbo Wan[1], Baohu Wu[2], Lei Hou[1] and Peiyi Wu[1]**

1. State Key Laboratory for Modification of Chemical Fibers and Polymer Materials, College of Chemistry and Chemical Engineering, Donghua University, Shanghai 201620, China

E-mail: wupeiyi@dhu.edu.cn; houlei@dhu.edu.cn

2. Jülich Centre for Neutron Science (JCNS) at Heinz Maier-Leibnitz Zentrum (MLZ) Forschungszentrum Jülich, Lichtenbergstr. 1, 85748 Garching, Germany

Keywords: tough hydrogel; solvent exchange; annealing; amphibious; polyvinyl alcohol

Abstract

Herein, we report the fabrication of amphibious polymer materials with outstanding mechanical performances, both underwater and in the air. A polyvinyl alcohol/poly(2-methoxyethylacrylate) (PVA/PMEA) composite with multiscale

nanostructures was prepared by combining solvent exchange and thermal annealing strategies, which contributed to nanophase separation with rigid PVA-rich and soft PMEA-rich phases and high-density crystalline domains of PVA chains, respectively. Benefiting from the multiscale nanostructure, the PVA/PMEA hydrogel demonstrated excellent stability in harsh (such as acidic, alkaline, and saline) aqueous solutions, as well as superior mechanical behavior with a breaking strength of up to 34.8 MPa and toughness of up to 214.2 MJ m^{-3}. Dehydrating the PVA/PMEA hydrogel resulted in an extremely robust plastic with a breaking strength of 65.4 MPa and toughness of 430.9 MJ m^{-3}. This study provides a promising phase–structure engineering route for constructing high-performance polymer materials for complex load-bearing environments.

1. Introduction

As 3D polymer networks swell in water, hydrogels exhibit excellent adaptability and flexibility, holding significant potentials in fields such as tissue engineering,[1] drug delivery,[2] soft robots,[3] wearable electronics,[4] energy-harvesting devices.[5] Conventional synthetic hydrogels are relatively weak and fragile, which hinders their application as load-bearing materials in machines and devices. Over the past few decades, tremendous efforts have been made to improve the mechanical performance of hydrogels, including double-network hydrogels,[6] nanocomposite hydrogels,[7] topological hydrogels[8] and dual-crosslinked hydrogels.[9] Recently, a facile soaking strategy[10] that does not involve complex molecular engineering was developed to strengthen and toughen hydrogels, accompanied by solvent exchange [11] or salting out[12] processes. Qiu et al.[13] developed a strong and antiswelling hydrogel by regulating intra- and interpolymer interactions based on exchanging a good solvent with a poor solvent. He et al.[14] produced a highly tough hydrogel with multi-length-scale hierarchical architecture using a freezing-assisted salting-out treatment. However, owing to the risk of noncovalent interaction alteration or salt leakage,

the mechanical performance of these hydrogels can easily deteriorate in external aqueous environments. Under such circumstances, developing a simple method to achieve high-performance hydrogels with excellent toughness and stability is challenging.

Hydrogels inevitably lose water when stored in the air and become brittle, which seriously restricts their application. Current strategies to solve this problem primarily focus on antidehydration hydrogels, which rely on the incorporation of different additives, such as water-miscible nonvolatile organic solvents[15] and highly hydratable salts[16] in hydrogel networks or encapsulation of hydrogels with hydrophobic elastomers.[17] However, the introduction of organic solvents or hygroscopic salts not only alters the inherent properties of hydrogels but also affects their long-term stability in water. In addition, hydrogel encapsulation complicates the fabrication process and causes interfacial problems. Inspired by amphibious animals[18] that demonstrate excellent adaptability to move and survive in both aquatic and terrestrial environments, this study provides an effective way to overcome the aforementioned issue by developing amphibious materials with high toughness in both hydrated and dehydrated states.

In this study, we propose a monomer-induced phase separation combined with a thermal annealing strategy to achieve amphibious polymer materials with extremely high strength and toughness in various aqueous solutions (acidic, alkaline, and salty) and in air. Herein, polyvinyl alcohol (PVA), a semicrystalline polymer with abundant pendent hydroxyl groups, was selected to construct the hydrophilic hard phase, whereas poly(2-methoxyethylacrylate) (PMEA), a biocompatible elastomer with ester and ether groups in the repeat unit, contributed to the hydrophobic soft phase. First, the PVA organogel was immersed in the monomer 2-methoxyethylacrylate (MEA) to induce a solvent-exchange process, where phase separation occurs with PVA chains shrinking considerably and consequently forming crystalline domains owing to the remarkable immiscibility of MEA with PVA. This phase separation can be arrested by the polymerization of MEA into PMEA, leading to a tough PVA/PMEA interpenetrating network. Thermal annealing was performed to further increase

the crystallinity of the PVA network, followed by equilibration in water. The synergy between high crystallinity and nanoscale phase separation afforded an antiswelling hydrogel with extreme stability in harsh aqueous solutions in the presence of strong acids, bases, and inorganic salts. The hydrogel demonstrated outstanding mechanical performance with a tensile breaking stress of up to 34.8 MPa and a fracture toughness of up to 214.2 MJ m^{-3}. Notably, a supertough plastic could be achieved with a tensile breaking stress of up to 65.4 MPa and fracture toughness of up to 430.9 MJ m^{-3} after dehydration of the hydrogel, demonstrating the considerable adaptability of such material in various environments. This study provides a practical method for fabricating amphibious polymer materials with high toughness in various aquatic and atmospheric environments for diverse applications.

2. Results and Discussion

2.1 Preparation of strong and tough PVA/PMEA composite

A PVA/PMEA composite with high strength and toughness was constructed using a sequential monomer-induced phase separation and annealing process, as depicted in **Figure 1a.** MEA, a liquid acrylate monomer that is strongly incompatible with PVA, was selected as the solvent exchange medium to induce the collapse of PVA in the organogel from a loose conformation into a dense one, accompanied by the formation of crystal domains. Dimethyl sulfoxide (DMSO) is a good solvent for PVA, and direct exchange of the PVA solvent from DMSO to MEA leads to abrupt macroscopic phase separation (Figure S1), which is unfavorable for obtaining highly robust materials with even structures. Under these circumstances, PVA organogels constructed from a binary solvent system composed of a good solvent (DMSO) and poor solvent (*N,N*-Dimethylformamide, DMF) were used for solvent exchange. PVA organogels are used owing to the following advantages: (1) the PVA/DMSO/DMF organogels are mechanically robust (Figure S2), which prevents the deformation of the samples during solvent exchange, and (2) the presence of DMF in the

organogel makes the phase transition gentle, leading to a shrunken transparent PVA/MEA composite (Figure S3).

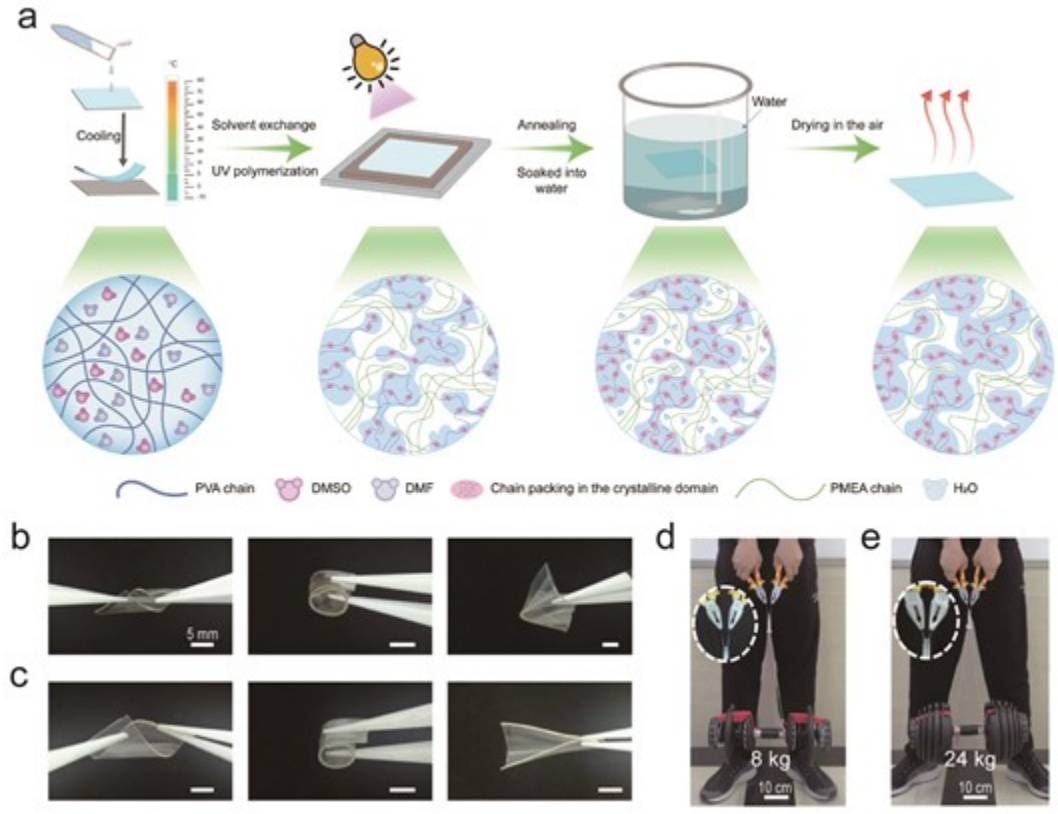

Figure 1. (a) Preparation of amphibious PVA/PMEA; Demonstration of the flexibility of PVA/PMEA hydrogel (b) and plastic (c); Demonstration of the lifting of weights by PVA/PMEA hydrogel (d) and plastic (e).

After solvent switching, *in-situ* polymerization of MEA in PVA/MEA was performed, affording a strong and tough PVA/PMEA interpenetrating network. The PVA/PMEA is afterward annealed under a pressure of 10 MPa at 100 ^{o}C, a temperature between the glass transition and melting temperature of PVA,[19] to initiate further PVA crystal growth and improve the crystallinity. Finally, a transparent PVA/PMEA hydrogel was obtained by swelling the annealed PVA/PMEA in water to equilibrium. Owing to the synergetic

integration of the crystalline PVA domains and hydrophobic PMEA networks, the hydrogel exhibited excellent antiswelling properties, outstanding flexibility, and high strength (Figure 1b and d). Furthermore, a super-strong and tough plastic was achieved after dehydration of the PVA/PMEA hydrogel in the air (Figure 1c and e), demonstrating the amphibious nature of the material.

2.2 Contribution of solvent-exchange and annealing to the mechanical performance

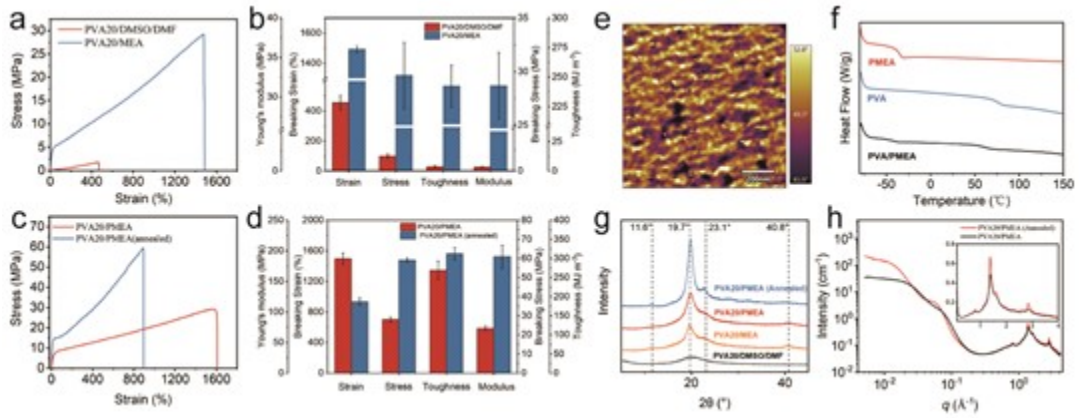

Figure 2. (a) Tensile stress–strain curves and (b) comparison of mechanical parameters before (PVA20/DMSO/DMF) and after (PVA20/MEA) solvent-exchange; (c) Tensile stress–strain curves and (d) comparison of mechanical parameters of PVA20/PMEA before and after annealing. (e) AFM phase image of PVA20/PMEA; (f) DSC curves of PMEA, PVA, and PVA20/PMEA; (g) X-ray diffraction (XRD) profiles during solvent-exchange and thermal annealing; (h) 1D SAXS/WAXS profiles of PVA20/PMEA before and after annealing.

Tensile tests were conducted to evaluate the effects of solvent exchange and thermal annealing on mechanical performance. As shown in **Figure 2a** and b, after immersing the PVA/DMSO/DMF organogel in MEA to an equilibrium, the tensile modulus (E) increases from 0.5 to 31.4 MPa, breaking strength (σ_b) increases from 1.7 to 29.6 MPa, breaking strain (ε_b) increases from 455% to 1492%, and toughness increases from 3.8 to 242.4 MJ m^{-3},

demonstrating the contribution of the solvent-exchange process to the significantly improved mechanical properties. Then, tough PVA/PMEA composites could be achieved after polymerizing MEA into PMEA, where the microstructure obtained during the solvent exchange process could be fixed. As the concentration of PVA in the original organogel increases, σ_b shows an increase from 13.2 to 34 MPa, while ε_b shows an optimized value of 16 for PVA20/PMEA ("20" implies that the concentration of PVA in the original organogel is 20 g per 100 mL DMSO/DMF) (Figure S4). Figure 2c and d indicate that annealing of the PVA20/PMEA composite at 100 ^{o}C and 10 MPa for 2 h leads to the notably increased E and σ_b. From these points of view, solvent exchange and thermal annealing contribute significantly to the mechanical performance of PVA/PMEA composites.

The solvent-exchange strategy has been widely used to achieve homogeneously crosslinked gel networks by finetuning the noncovalent interactions.[20] Herein, with the exchange of a relatively good solvent (DMSO/DMF binary system) with an extremely poor solvent (MEA), the PVA chains experienced a conformational change from the relatively extended to collapsed ones accompanied by enhanced intra- and interpolymer interactions, finally resulting in a phase-separated network composed of PVA-rich and MEA-rich phases. Such phase separation was immobilized by polymerizing MEA into PMEA. To validate the phase-separation structure of the PVA/PMEA, atomic force microscopy (AFM) was employed to obtain phase images of the composite after polymerization. In Figure 2e, the bright areas indicate regions of relatively high modulus (PVA-concentrated phase of crystalline domains), and dark areas correspond to regions of relatively low modulus (PVA-dilute phase of amorphous domains).[21] PVA20/PMEA had a homogeneous nanophase-separated structure with a length scale much smaller than the wavelength of visible light, which contributed to the transparency and toughness of the composite. With increasing PVA content, the AFM phase image shows more intense bright areas (Figure S5), which is consistent with the increase in modulus at higher PVA content. The phase-separated structure of PVA20/PMEA was verified using differential scanning calorimetry (DSC)

measurement. As shown in Figure 2f, two glass transition temperatures are identified in the DSC curve of PVA/PMEA, where the higher T_g (61 ^oC) is related to the rigid region of the PVA-rich phase while the lower one (-47 ^oC) corresponds to the soft region mainly composed of PMEA chains. The PVA-rich phase strengthened the composite by forming dense hydrogen bonds between the PVA chains, whereas the PMEA-rich phase was highly flexible to enable large strains, synergistically toughening the composite.

In addition to its phase separation structure, PVA is a typical semicrystalline polymer, and the collapsed PVA chains in the PVA-rich phase result in the formation of crystal domains, further promoting the mechanical robustness of the PVA/PMEA composite. X-ray diffraction (XRD) was performed to study the crystalline structures of the PVA-based materials during solvent exchange and annealing. As shown in Figure 2g, the diffraction peak at $2\theta = 19.7^o$, originating from the typical reflection plane of $(10\bar{1})$ in semicrystalline PVA, exhibits an abrupt intensification after solvent replacement with MEA. Moreover, small peaks at $2\theta = 11.6^o$, 23.1^o, and 40.8^o, which are absent in the organogel, come into being after solvent exchange. The peaks at 11.6^o, 23.1^o, and 40.8^o in the XRD pattern are attributed to the (100), (200), and (102) planes of the PVA crystalline structure, respectively.[12b, 20c] Under such a circumstance, we inferred that the phase separation upon solvent exchange is accompanied by crystal domain formation within PVA chains. After the polymerization of the MEA, the XRD profile remained approximately the same, suggesting that the crystalline structure did not interfere with polymerization. Thermal annealing effectively enhances the mechanical performance of PVA-based hydrogels by tuning the crystallinity and optimizing the crystallization domain. Figure 2g and Figure S6 demonstrate that the PVA/PMEA composites exhibit an increased crystallinity after annealing, which is responsible for the improved E and σ_b in Figure 2c. Furthermore, the microstructure of PVA/PMEA after annealing was investigated using small-angle X-ray scattering (SAXS) and wide-angle X-ray scattering (WAXS). As shown in Figure 2h, in the SAXS range ($q < 0.5$ $Å^{-1}$), the step-like appearance of the scattering curves is attributed to the scattering from nanophase separation

(0.005-0.03 Å^{-1}) and crystalline domain (0.04-0.06 Å^{-1}), respectively. After annealing, the scattering related to the crystalline domain is significantly enhanced. The distinct plateau shape of the scattering curve indicates that the PVA crystalline domains are relatively isolated compared with the continuous structures. Annealing also increases the size (diameter) of the crystalline domains from ~7 to 8.5 nm. In addition, the WAXS results (q > 0.5 Å^{-1}) showed a significant increase in the crystallinity of the samples after annealing. Hence, the SAXS/WAXS results demonstrate that annealing enhances the crystallinity of PVA and promotes the formation of dense discrete crystalline domains.

.3 Properties and structures of PVA/PMEA hydrogels

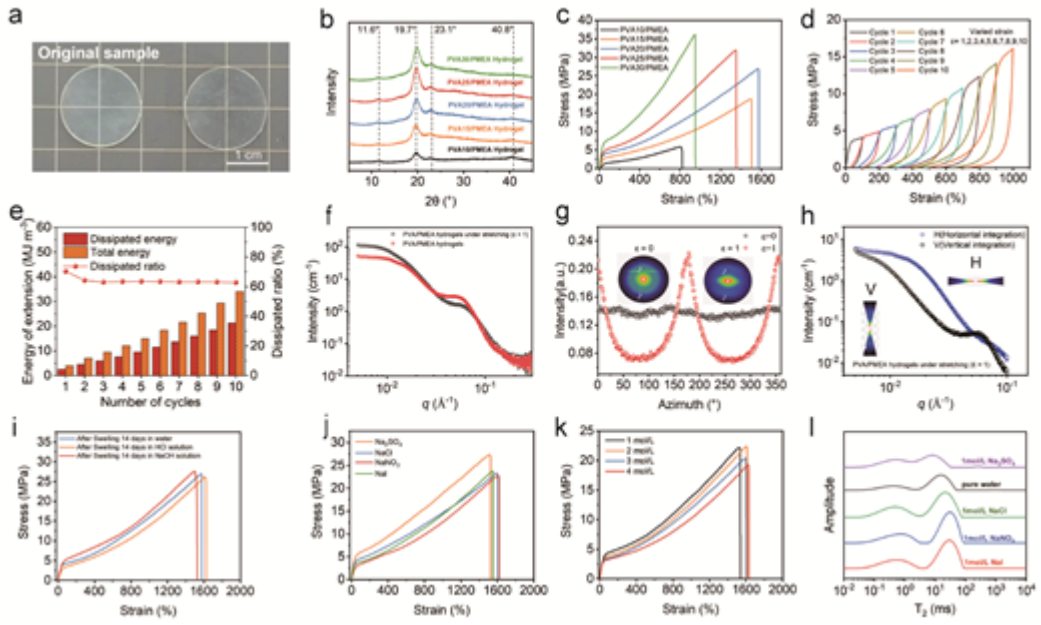

Figure 3. (a) Images of PVA20/PMEA before (left) and after (right) swollen in water; (b) XRD profiles of PVA/PMEA hydrogels; (c) Tensile stress–strain curves of PVA/PMEA hydrogels; (d) Sequential loading–unloading tensile tests without interval and (e) the corresponding calculated total and dissipated energy as well as dissipated ratio of the PVA20/PMEA hydrogels under different strains (ε = 1–10);

(f) 1D SAXS profiles of PVA20/PMEA hydrogels under stretching (ε = 1); (g) 2D SAXS profiles and azimuthally-integrated SAXS data of PVA20/PMEA hydrogels under stretching (ε = 1); (h) Horizontal and vertical integrated SAXS profiles of PVA20/PMEA hydrogels under stretching (ε = 1); Tensile stress–strain curves of PVA20/PMEA hydrogels in various aqueous solutions: acid and alkaline (i), salty (j), and $NaNO_3$ of different concentrations (k); (l) LF-^{1}H NMR curves of PVA20/PMEA hydrogels in various aqueous solutions.

The PVA/PMEA hydrogels were obtained by immersing the PVA/PMEA composites in deionized water until equilibrium was reached. Most hydrogels inevitably exhibit dramatic swelling after soaking in water, which inherently deteriorates their mechanical performance and consequently hinders their applications.[22] The PVA/PMEA composite exhibited excellent antiswelling behavior with negligible changes in volume after swelling in water to equilibrium (**Figure 3a**), which might be due to the high-density crystalline domains of the PVA and hydrophobic PMEA segments. The water content was between 33 and 45 wt% after being fully swollen in water (Figure S7). The XRD patterns (Figure 3b) confirmed that the crystalline structure was barely affected by the presence of water and retained in the PVA/PMEA hydrogels. The mechanical properties of the PVA/PMEA hydrogels with various PVA contents were studying using tensile tests, and the corresponding stress–strain curves are shown in Figure 3c. Owing to the absence of drastic swelling, the PVA/PMEA hydrogels are strong and tough with E of 3.9 to 23.5 MPa, σ_b ranging from 5.9 to 34.8 MPa, and toughness up to 214.2 MJ m^{-3} (Figure S8). In PVA/PMEA hydrogels, PVA chains dominate the E and σ_b, while PMEA chains mainly contribute to the stretchability. From this point of view, increasing the PVA content in the hydrogel would lead to increased E and σ_b and decreased ε_b, which is consistent with the mechanical performance of the hydrogel at relatively high PVA content. At a low PVA content, the crystalline domains of the PVA chains homogeneously distributed in the hydrogel acted as robust and dynamic crosslinking points, which restricted the deformation of the hydrogel network at the initial stage of

deformation and gradually dissociated to dissipate energy at large strains.[20c] Thus, increasing the PVA content in the hydrogel leads to simultaneously increased E, σ_b, ε_b, and toughness.

PVA20/PMEA hydrogel demonstrates the optimized elongation with high σ_b, which will be used for further study. Energy dissipation of the PVA20/PMEA hydrogel was investigated using continuous cyclic tensile loading at various stretch ratios. As demonstrated in Figure 3d and e, when increasing the tensile strain from 1 to 10 without pausing between each cycle, the dissipated energy of PVA20/PMEA hydrogel increases from 2.6 to 21.4 MJ m^{-3}, and the corresponding dissipation ratios are rather high, indicating efficient energy dissipation to toughen the hydrogels. SAXS measurements were performed to investigate the microstructural evolution of PVA20/PMEA hydrogels. As shown in Figure 3f, the scattering curves can be attributed to scattering from the nanophase separation and PVA-dominated crystalline domain, which is consistent with the situation of the PVA/PMEA composite before it swells in water. From this perspective, the hydrogels retained both their nanophase-separated structures and crystalline domains. In addition, the 2D SAXS elongated patterns and corresponding azimuth plots (Figure 3g) indicate that the nanophase separation structure in the hydrogels became oriented upon stretching. The integration results along the direction perpendicular to the stretching direction (direction H) and along the stretching direction (direction V) shown in Figure 3h demonstrate the presence of different components in the hydrogels under stretching. The findings reveal that stretching significantly increases the size of the nano-separated phase, while the nanocrystalline phase remains unaffected by stretching at $\varepsilon = 1$. Under such circumstances, it can be deduced that the soft PMEA-rich phase was adaptive and contributed dominantly to elongation.

Furthermore, the stability of the PVA/PMEA hydrogels in harsh environments, including strongly acidic, alkaline, and saline environments, was explored. As shown in Figure S9, the PVA20/PMEA hydrogels were nearly transparent without obvious volume changes after immersion in 1 M HCl, NaOH, and various salt aqueous solutions for 7 d,

indicating that the microstructure was barely or only slightly influenced by the presence of diverse ions. Figure 3i and j show the tensile stress–strain curves of the PVA20/PMEA hydrogels in different aqueous environments, where the mechanical properties were similar to those in pure water. The hydrogels remain highly strong and tough with σ_b in the range of 22.5–27.3 MPa and toughness between 179.5 and 233.9 MJ m^{-3}, indicating that the mechanical performance of PVA20/PMEA hydrogel is less disturbed by acidic, alkaline or saline environments (Figure S10). Herein, the hydrogel in the Na_2SO_4 aqueous solution exhibits a slightly better mechanical performance, which might be caused by the "salting-out" effect of SO_4^{2-} on the PVA chains in the amorphous region. In addition, the tensile behavior of the hydrogel remained nearly unchanged even in 4 M $NaNO_3$ (Figure 3k and S11), further demonstrating its excellent stability against high salt concentrations. In traditional hydrogel networks, the mechanical performance is seriously influenced, either improved or weakened, by the presence of ions, mainly owing to the Hofmeister or ion-specific effects.[23] The impact of different ions on the hydration water around polymer chains plays an important role in determining ionic specificity.[24] The Low-field-^{1}H nuclear magnetic resonance (LF-^{1}H NMR) involves the measurement of the spin–spin relaxation time of protons and is a suitable method for studying the state of water molecules in aqueous systems.[25] In Figure 3l, the two bands recognized in the curves could be related to protons in the polymer chains and water molecules from low T_2 to high T_2. Meanwhile, the T_2 of water molecules in the hydrogel was less affected by various ions and was mainly located in the range of 10–100 ms, indicating that water molecules in the hydrogel were moderately mobile despite the presence of different ions. Under such circumstances, water molecules are always moderately hydrogen-bonded with polymer chains in confined regions owing to the coexistence of the hydrophobic PMEA-rich phase and crystalline PVA-rich phase, which benefits the high stability of the PVA/PMEA hydrogel under various harsh aqueous conditions. The XRD patterns (Figure S12) further confirm that the crystalline structure of the PVA chains was hardly disturbed in acidic, alkaline, or saline aqueous solutions. In addition, the

PVA20/PMEA hydrogel was resistant to reductive and oxidative conditions, and its mechanical performance remained similar to that in pure water (Figure S13).

2.4 Properties and structures of PVA/PMEA plastics

A strong and tough PVA/PMEA plastic can be easily achieved after air-drying the PVA/PMEA hydrogel. As shown in **Figure 4a** and b, the dehydration of PVA20/PMEA hydrogel induced significantly enhanced mechanical properties, affording a dried plastic with E of 669.2 MPa, σ_b of 65.4 Mpa, and toughness of 430.9 MJ m^{-3}. The mechanical performance was much better than that of the PVA/PMEA composite before soaking in water, which was due to the removal of organic solvent residues. Notably, the toughness is even higher than the toughest spider silk (*ca.* 383 MJ m^{-3}) ever found in the world.[26] Moreover, the mechanical performance was highly reversible during cyclic dehydration and hydration processes (Figure 4c). Water molecules have a plasticizing effect on the polymer chains in the plastic, which is mainly achieved through the hydrophobic hydration of C–H groups as well as the hydrogen bonding of C–OH/C–O–C groups with water, as indicated by the FTIR spectra of the PVA20/PMEA plastic before and after hydration (Figure S14). The microstructure of PVA20/PMEA plastic was investigated to study the toughening mechanism. The XRD profile indicates that the plastic was highly crystalline (~43.6%, Figure S15). The DSC curve (Figure S16) of the PVA20/PMEA plastic shows a pronounced melting peak at ~230 ^{o}C, confirming the crystalline structure within the plastic. Furthermore, two T_g values were observed in the DSC curve, indicating the phase-separated structure of the plastic. Despite the glass transition of PVA in the amorphous region, the plastic remained highly stiff below ~150 ^{o}C (Figure S17) owing to the presence of high-density crystalline domains. In addition, multiscale structures with both nanophase separation and crystalline domains of the plastic can be deduced from the SAXS curve shown in Figure S18. Thus, the coordination of nanophase separation and crystalline domain endows the PVA/PMEA plastic with outstanding mechanical performance, where the hard PVA-rich phase and soft PMEA-rich phase in the nanophase-separated structure favor high strength and stretchability,

respectively, and the high-density crystalline domains are beneficial for further stiffening and strengthening the plastic.

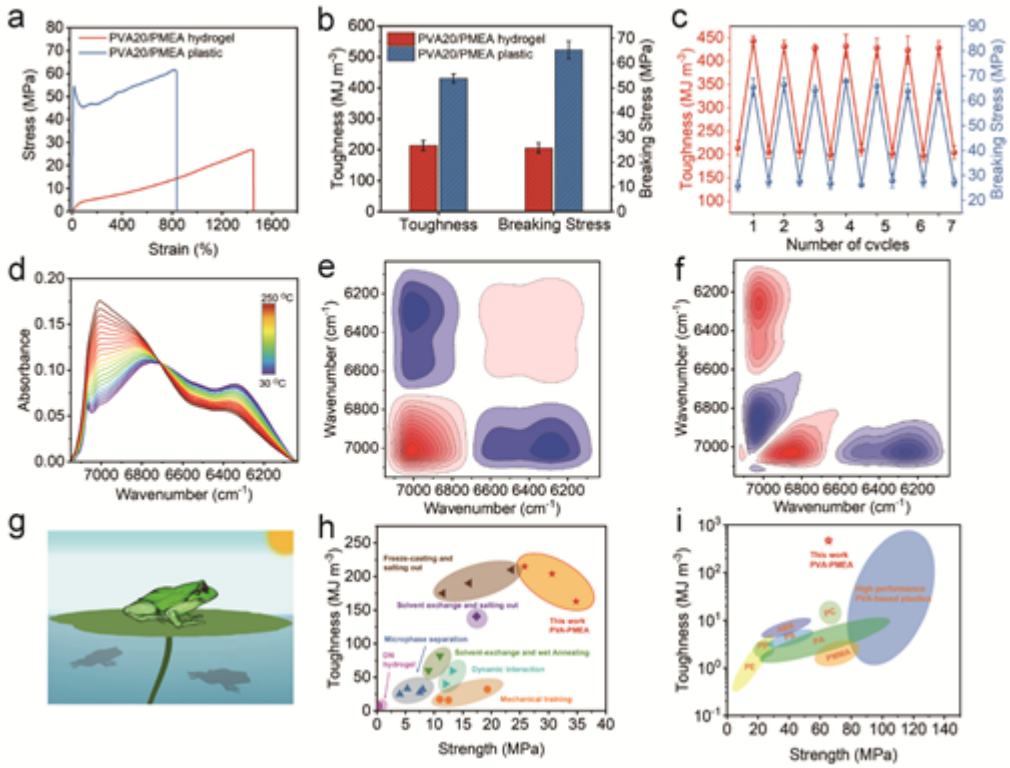

Figure 4. (a) Tensile stress–strain curves and (b) comparison of mechanical parameters of PVA20/PMEA hydrogel and plastic; (c) Mechanical parameters during cyclic dehydration and hydration processes; (d) Temperature-dependent NIR spectroscopy of PVA20/PMEA plastic; 2Dcos synchronous (e) and asynchronous (f) maps of PVA20/PMEA plastic during heating; (g) Image showing the amphibious animal adaptable in both underwater and terrestrial regions; Comparison of the mechanical performance of the PVA/PMEA hydrogel (h) and plastic (i) with the current state-of-the-art polymer materials (double network,[27] dynamic interaction,[28] mechanical training,[29] microphase separation,[30] olvent-exchange and salting-out,[20c] solvent-exchange and wet-annealing,[31]

freeze-casting and salting-out,[14] high-performance PVA-based plastics,[15b, 32] common commercial plastics[33]).

Hydrogen bonding between PVA chains plays a vital role in forming multiscale microstructures and predominantly contributes to energy dissipation upon stretching. Temperature-dependent near-infrared (NIR) spectroscopy was employed to validate the hydrogen-bonding interactions within the PVA chains responsible for the mechanical robustness of the PVA/PMEA plastics (Figure 4d). The NIR region is dominated by overtone and combination vibrations related to groups containing hydrogen atoms, such as O–H, N–H, and C–H. In addition, NIR spectroscopy has the advantages of rapid and nondestructive analysis of bulk materials with easy sample preparation. Herein, we mainly focus on the bands in the region between 7150 and 6030 cm^{-1}, which can be assigned to the first overtone of O–H stretching in the PVA chains. During the entire heating process, the band exhibited a bidirectional spectral intensity change, with the intensity of the bands at lower wavenumbers decreasing and those at higher wavenumbers increasing, indicating the transformation of strongly hydrogen-bonded OH groups to weakly hydrogen-bonded ones. Moreover, it is observed that a relatively sharp peak located at 7070 cm^{-1} exists in this region and gradually becomes weak upon heating. To figure out the origin of this peak, NIR spectra of PVA-based samples under different treatments are compared in the 7200–6300 cm^{-1} region (Figure S19). The peak at 7070 cm^{-1} appears after the solvent exchange of DMSO/DMF with MEA and becomes more evident after thermal annealing. However, a peak remained for the PVA/PMEA hydrogel. By comparison with the XRD results, we deduce that the peak at 7070 cm^{-1} appears and changes with the crystalline structures of the PVA chains, and thus tentatively corresponds to ordered OH groups in the crystalline domains. The variation in this peak upon heating reflects a reduction in the ordered crystalline structures. Two-dimensional correlation spectra (2Dcos, Figure 4e and f) were generated from the temperature-variable NIR spectra to identify the fine structures in the PVA chains and discern the change sequence of different OH species.[34] In the asynchronous map, three subtle bands at 7031, 6858, and

6256 cm^{-1} were observed, which could be related to ordered OH in the crystalline domains, weakly hydrogen-bonded OH, and strongly hydrogen-bonded OH, respectively, providing details on the internal interactions of the PVA chains. In addition, the variation order of OH groups in different states upon heating could be determined based on Noda's rule,[35] which is described as follows: 6256 → 7031→ 6858 cm^{-1} ("→" means before or earlier to). This sequence highlights the weakening or breaking of hydrogen bonds between PVA chains during the entire heating process. In addition, the change in hydrogen bonding occurred before the decrement in ordered OH groups, further confirming the dominant contribution of hydrogen bonding to the crystalline domains.

Hydrogels inevitably suffer from water evaporation when stored in air and finally lose flexibility, which seriously inhibits their practical use. Current strategies to solve this problem mainly focus on the retention of water molecules by adding nonvolatile organic compounds with strong water-absorbing abilities or highly hydratable salts, which reduce their stability in aqueous environments owing to the leakage of organic compounds or salts. Herein, PVA/PMEA exhibits high mechanical performance in both hydrated and dehydrated states, resembling amphibious animals adaptable to underwater and terrestrial regions (Figure 4g). Moreover, a conflict exists between the strength and toughness of polymer materials, which is overcome in our work by introducing a nanophase-separated structure with both stiff and soft phases, as well as a high density of crystalline domains in the stiff phase. Consequently, both the PVA/PMEA hydrogel and plastic simultaneously show high strength and toughness, which are superior to or comparable to the current state-of-the-art polymer materials (Figure 4h and i).

3. Conclusion

In summary, we report a highly adaptable polymer composite with remarkable strength and superior toughness in various harsh (acidic, alkaline, and saline) aqueous environments as well as under atmospheric conditions, demonstrating significant potential as a load-bearing

material in complex environments. Combining monomer-induced solvent exchange and compression-assisted thermal annealing, a PVA/PMEA composite with multiscale nanostructures was achieved with outstanding mechanical performance. Particularly, the solvent exchange from a relatively good solvent system (DMSO/DMF) of PVA to an extremely poor one (MEA) resulted in nanophase separation composed of PVA-rich and MEA-rich phases, which could be arrested by the polymerization of MEA. Thermal annealing of the PVA/PMEA between the glass transition and melting temperatures of PVA led to significantly increased crystallinity. Owing to the synergetic effect of the high-density crystalline PVA-rich phase and hydrophobic soft PMEA-rich phase, the PVA/PMEA hydrogel not only exhibited excellent stability in various aqueous solutions but also demonstrated mechanical performance with a breaking strength of 34.8 MPa and toughness up to 214.2 MJ m^{-3}. Moreover, dehydrating the PVA/PMEA hydrogel afforded a robust plastic with a breaking strength of 65.4 MPa and toughness of 430.9 MJ m^{-3}. This study provides a practical method for phase structure engineering to fabricate amphibious polymer materials with superior strength and toughness in various aquatic and atmospheric environments for diverse load-bearing scenarios.

4. Experimental Section

4.1 Materials

Polyvinyl alcohol (PVA, M.W. 146,000-186,000, 98% hydrolysis) was purchased from Sigma-Aldrich. 2-methoxyethylacrylate (MEA) was purchased from TCI Chemical and purified by passing it through an alumina column. Dimethyl sulfoxide (DMSO) and dimethyl formamide (DMF) were obtained from Adamas-Beta. 2,2-Diethoxyacetophenone (DEAP) was purchased from TCI Chemical. Hydrochloric acid (HCl), sodium hydroxide (NaOH), sodium sulfate (Na_2SO_4), sodium chloride (NaCl), sodium nitrate ($NaNO_3$) and sodium iodide (NaI) were purchased from Sinopharm Chemicals.

4.2 Preparation of PVA organogels

PVA organogels with different compositions was prepared using a simple cooling process. First, PVA was added into the mixture of DMSO and DMF with the volume ratio of DMSO to DMF fixed at 6:4, followed by stirring continuously at 90 ^{o}C for 8 h. The concentrations of PVA were 10, 15, 20, 25, and 30 g per 100 mL of the mixed solvents. Then, the PVA solutions were injected into a PTFE mold sandwiched between two glass sheets in an oven at 80 ^{o}C. The heater was then turned off, allowing the samples to cool naturally to room temperature within 8 h. Finally, the PVA organogels were obtained by refrigerating at 4 ^{o}C for 12 h.

4.3 Preparation of PVA/PMEA hydrogel and corresponding plastic

The prepared PVA organogels were immersed directly in MEA for 24 h for solvent exchange and then replaced with MEA containing 1 wt% DEAP for another 48 h in the dark, allowing the initiator to diffuse into the gel. After curing under 365 nm UV light for 30 min, PVAX/PMEA composites were obtained ("X" means that the concentration of PVA in the original organogel is X g per 100 mL DMSO/DMF). Furthermore, the PVA/PMEA composites were annealed in a stainless-steel mold consisting of two sheets and one skeletonized frame at 100 ^{o}C and 10 MPa for 2 h. Finally, the PVA/PMEA hydrogels were prepared by soaking the annealed PVA/PMEA in pure water for 48 h to reach equilibrium. In addition, the PVA/PMEA plastic was easily obtained after air-drying the PVA/PMEA hydrogel.

4.4 Characterizations

Tensile tests were performed on a universal testing machine (UTM2103, Shenzhen Suns Technology) with the samples cut into a dumbbell shape and at a stretching rate of 10 min^{-1}. Atomic force microscopy (AFM) images were obtained using an MFP3D Bio instrument (Oxford). Differential scanning calorimetry (DSC) curves were collected using TA DSC250 in the temperature range between -80 and 250 °C with a scanning rate of 20 °C min^{-1} (nitrogen flow). XRD profiles were obtained using an 18-kW rotating-target X-ray

diffractometer (D/MAX-2550VB, Rigaku). Low-field nuclear magnetic resonance (LF-NMR) measurements were performed using a VTMR20-010V-I NMR analyzer (Suzhou Niumag Corporation, China). The water contents, q, of the hydrogels were calculated using $q = \frac{(w_s - w_d)}{w_s} \times 100\%$, where w_s and w_d are the mass of hydrogels in swollen and dried states, respectively.

SAXS and WAXS experiments were conducted at the JCNS MLZ using the laboratory-based SAXS-WAXS beamline KWS-X (XENOCS XUESS 3.0 XL). A MetalJet X-ray source (Excillum D2+) with a liquid metal anode operated at 70 kV and 3.57 mA, emitting Ga-Kα radiation with a wavelength (λ) of 1.314 Å. The 2D scattering data from the stretched sample were integrated along both the stretching direction and perpendicular to it, resulting in 1D data.

The temperature-dependent NIR spectra were collected on a Nicolet iS50 spectrometer at a heating rate of 2 ^{o}C min^{-1} between 30 and 250 ^{o}C. 2D correlation spectroscopy (2Dcos) analysis was performed using 2D Shige ver. 1.3 (Shigeaki Morita, Kwansei-Gakuin University, Japan, 2004-2005) and plotted onto contour maps using Origin ver. 9.8, where warm colors (red) indicate positive intensities and cool colors (blue) represent negative intensities.

Supporting Information

Supporting Information is available from the Wiley Online Library or from the author.

Acknowledgements

The authors gratefully acknowledge the financial support of the National Natural Science Foundation of China (NSFC) (Nos. 51973035, 52161135102).

.

References

[1] a)Y. Yang, Z. Yu, X. Lu, J. Dai, C. Zhou, J. Yan, L. Wang, Z. Wang, J. Zang, *Bioact. Mater.* **2023**, 26, 465; b)M. Sun, H. Li, Y. Hou, N. Huang, X. Xia, H. Zhu, Q. Xu, Y. Lin, L. Xu, *Sci. Adv.* **2023**, 9, eade6973.

[2] a)X. Fu, L. Hosta-Rigau, R. Chandrawati, J. Cui, *Chem* **2018**, 4, 2084; b)J. Liao, H. Huang, *Biomacromolecules* **2020**, 21, 2574.

[3] a)Y. Chi, Y. Hong, Y. Zhao, Y. Li, J. Yin, *Sci. Adv.* **2022**, 8, eadd3788; b)G. Gu, N. Zhang, C. Chen, H. Xu, X. Zhu, *ACS Nano* **2023**, 17, 9661.

[4] a)B. Ying, X. Liu, *iScience* **2021**, 24, 103174; b)M. Tan, Y. Xu, Z. Gao, T. Yuan, Q. Liu, R. Yang, B. Zhang, L. Peng, *Adv. Mater.* **2022**, 34, 2108491.

[5] a)Y. Wang, L. Zhang, A. Lu, *J. Mater. Chem. A* **2020**, 8, 13935; b)X. Luo, L. Zhu, Y. C. Wang, J. Li, J. Nie, Z. L. Wang, *Adv. Funct. Mater.* **2021**, 31, 2104928.

[6] a)X. Zhang, H. Geng, X. Zhang, Y. Liu, J. Hao, J. Cui, *J. Mater. Chem. A* **2023**, 11, 2996; b)J. Wu, Z. Wu, H. Xu, Q. Wu, C. Liu, B.-R. Yang, X. Gui, X. Xie, K. Tao, Y. Shen, J. Miao, L. K. Norford, *Mater. Horiz.* **2019**, 6, 595.

[7] a)X. Meng, Y. Qiao, C. Do, W. Bras, C. He, Y. Ke, T. P. Russell, D. Qiu, *Adv. Mater.* **2022**, 34, 2108243; b)J. Hu, I. Altun, Z. Zhang, H. Albadawi, M. A. Salomao, J. L. Mayer, L. Hemachandra, S. Rehman, R. Oklu, *Adv. Mater.* **2020**, 32, 2002611.

[8] a)J. Kim, G. Zhang, M. Shi, Z. Suo, *Science* **2021**, 374, 212; b)C. Liu, N. Morimoto, L. Jiang, S. Kawahara, T. Noritomi, H. Yokoyama, K. Mayumi, K. Ito, *Science* **2021**, 372, 1078.

[9] a)C. Jiang, X. Ding, W. Xie, D. Wu, *ACS Appl. Mater. Interfaces* **2022**, 14, 55143; b)H. Fan, J. Wang, Z. Jin, *Macromolecules* **2018**, 51, 1696.

[10] Y. Yang, X. Wang, F. Yang, H. Shen, D. Wu, *Adv. Mater.* **2016**, 28, 7178.

[11] a)H. Zhang, N. Tang, X. Yu, M. H. Li, J. Hu, *Adv. Funct. Mater.* **2022**, 32, 22006305; b)T. Shu, K. Zheng, Z. Zhang, J. Ren, Z. Wang, Y. Pei, J. Yeo, G. X. Gu, S. Ling, *Biomacromolecules* **2021**, 22, 1955.

[12] a)H. Zou, X. Meng, X. Zhao, J. Qiu, *Adv. Mater.* **2023**, 35, 2207262; b)D. Liu, Y. Cao, P. Jiang, Y. Wang, Y. Lu, Z. Ji, X. Wang, W. Liu, *Small* **2023**, 19, 2206819.

[13] L. Xu, S. Gao, Q. Guo, C. Wang, Y. Qiao, D. Qiu, *Adv. Mater.* **2020**, 32, 2004579.

[14] M. Hua, S. Wu, Y. Ma, Y. Zhao, Z. Chen, I. Frenkel, J. Strzalka, H. Zhou, X. Zhu, X. He, *Nature* **2021**, 590, 594.

[15] a)Z. Han, P. Wang, Y. Lu, Z. Jia, S. Qu, W. Yang, *Sci. Adv.* **2022**, 8, eabl5066; b)X. Fang, Y. Qing, Y. Lou, X. Gao, H. Wang, X. Wang, Y. Li, Y. Qin, J. Sun, *ACS Mater. Lett.* **2022**, 4, 1132.

[16] Y. Jian, S. Handschuh-Wang, J. Zhang, W. Lu, X. Zhou, T. Chen, *Mater. Horiz.* **2021**, 8, 351.

[17] T. Zhu, C. Jiang, M. Wang, C. Zhu, N. Zhao, J. Xu, *Adv. Funct. Mater.* **2021**, 31, 2102433.

[18] Z. Cheng, W. Feng, Y. Zhang, L. Sun, Y. Liu, L. Chen, C. Wang, *Adv. Mater.* **2023**, 2301005.

[19] a)X. Liang, G. Chen, S. Lin, J. Zhang, L. Wang, P. Zhang, Z. Wang, Z. Wang, Y. Lan, Q. Ge, J. Liu, *Adv. Mater.* **2021**, 33, e2102011; b)X. Liang, G. Chen, I. M. Lei, P. Zhang, Z. Wang, X. Chen, M. Lu, J. Zhang, Z. Wang, T. Sun, Y. Lan, J. Liu, *Adv. Mater.* **2023**, 35, 2207587.

[20] a)Q. Zhang, H. Fan, L. Zhang, Z. Jin, *Macromolecules* **2020**, 53, 7025; b)B. Fang, J. Yan, D. Chang, J. Piao, K. M. Ma, Q. Gu, P. Gao, Y. Chai, X. Tao, *Nat. Commun.* **2022**, 13, 2101; c)L. Xu, Y. Qiao, D. Qiu, *Adv. Mater.* **2023**, 35, 2209913.

[21] S. Lin, X. Liu, J. Liu, H. Yuk, H. C. Loh, G. A. Parada, C. Settens, J. Song, A. Masic, G. H. McKinley, X. Zhao, *Sci. Adv.* **2019**, 5, eaau8528.

[22] H. Shan, P. Poredos, Z. Ye, H. Qu, Y. Zhang, M. Zhou, R. Wang, S. C. Tan, *Adv. Mater.* **2023**, 2302038.

[23] a)M. Zhang, Y. Yang, M. Li, Q. Shang, R. Xie, J. Yu, K. Shen, Y. Zhang, Y. Cheng, *Adv. Mater.* **2023**, 2301551; b)S. Han, Q. Wu, J. Zhu, J. Zhang, A. Chen, S. Su, J. Liu, J. Huang, X. Yang, L. Guan, *Mater. Horiz.* **2023**, 10, 1012.

[24] S. Wu, M. Hua, Y. Alsaid, Y. Du, Y. Ma, Y. Zhao, C. Y. Lo, C. Wang, D. Wu, B. Yao, J. Strzalka, H. Zhou, X. Zhu, X. He, *Adv. Mater.* **2021**, 33, 2007829.

[25] K. Gong, L. Hou, P. Wu, *Adv. Mater.* **2022**, 34, 2201065.

[26] W. He, D. Qian, Y. Wang, G. Zhang, Y. Cheng, X. Hu, K. Wen, M. Wang, Z. Liu, X. Zhou, M. Zhu, *Adv. Mater.* **2022**, 34, 2201843.

[27] J. Y. Sun, X. Zhao, W. R. Illeperuma, O. Chaudhuri, K. H. Oh, D. J. Mooney, J. J. Vlassak, Z. Suo, *Nature* **2012**, 489, 133.

[28] T. Shui, M. Pan, A. Li, H. Fan, J. Wu, Q. Liu, H. Zeng, *Chem. Mater.* **2022**, 34, 8613.

[29] C. Luo, M. Huang, X. Sun, N. Wei, H. Shi, H. Li, M. Lin, J. Sun, *ACS Appl. Mater. Interfaces* **2022**, 14, 2638.

[30] J. Wu, Z. Zhang, Z. Wu, D. Liu, X. Yang, Y. Wang, X. Jia, X. Xu, P. Jiang, X. Wang, *Adv. Funct. Mater.* **2022**, 33, 2210395.

[31] Y. Wu, Y. Zhang, H. Wu, J. Wen, S. Zhang, W. Xing, H. Zhang, H. Xue, J. Gao, Y. Mai, *Adv. Mater.* **2023**, 35, 2210624.

[32] a)Z. Ling, C. E. Ren, M. Q. Zhao, J. Yang, J. M. Giammarco, J. Qiu, M. W. Barsoum, Y. Gogotsi, *Proc. Natl. Acad. Sci. U. S. A.* **2014**, 111, 16676; b)Y. Guan, W. Li, Y. Zhang, Z. Shi, J. Tan, F. Wang, Y. Wang, *Compos. Sci. Technol.* **2017**, 144, 193; c)L. Shao, J. Li, Y. Guang, Y. Zhang, H. Zhang, X. Che, Y. Wang, *Mater. Des.* **2016**, 99, 235; d)X. Zhang, W. Liu, D. Yang, X. Qiu, *Adv. Funct. Mater.* **2019**, 29, 1806912; e)W. Niu, Y. Zhu, R. Wang, Z. Lu, X. Liu, J. Sun, *ACS Appl. Mater. Interfaces* **2020**, 12, 30805; f)L. Liu, M. Zhu, X. Xu, X. Li, Z. Ma, Z. Jiang, A. Pich, H. Wang, P. Song, *Adv. Mater.* **2021**, 33, 2105829.

[33] M. F. Ashby, in Materials and the Environment, 2nd ed. (Ed.: M. F. Ashby), Butterworth-Heinemann, Boston 2013, Ch. p. 15.

[34] Y. Wang, S. Sun, P. Wu, *Adv. Funct. Mater.* **2021**, 31, 2101494.

[35] L. Hou, P. Wu, *Acta. Polym. Sin.* **2022**, 53, 522.

A delicate nanostructure design with nanophase separation and crystalline domains leads to an amphibious polymer material with outstanding mechanical performance in both hydrated and dehydrated states, affording a hydrogel with a toughness of up to 214.2 MJ m^{-3} and a plastic with a toughness of up to 430.9 MJ m^{-3}. In addition, the hydrogel exhibits excellent stability in acidic, alkaline, and saline aqueous environments.

Hongbo Wan, Baohu Wu, Lei Hou and Peiyi Wu**

Amphibious Polymer Materials with High Strength and Superb Toughness in Various Aquatic and Atmospheric Environments